Science of the Total Environment xxx (2013) xxx–xxx

Contents lists available at SciVerse ScienceDirect

Science of the Total Environment

journal homepage: www.elsevier.com/locate/scitotenv

Concurrent photolytic degradation of aqueous methylmercury and dissolved organic matter

Jacob A. Fleck [a,*], Gary Gill [b], Brian A. Bergamaschi [a], Tamara E.C. Kraus [a], Bryan D. Downing [a], Charles N. Alpers [a]

[a] U.S. Geological Survey, California Water Science Center, 6000 J St., Placer Hall, Sacramento, CA 95819, USA
[b] Pacific Northwest National Laboratory, Marine Sciences Laboratory, 1529 West Sequim Bay Road Sequim, WA 98382, USA

HIGHLIGHTS

- MeHg photodegradation rates were similar in natural waters over a wide range of DOM.
- MeHg concentration was related to labile DOM but percent loss was related to humic DOM.
- Optical measurements of DOM could aid in monitoring in situ MeHg photodegradation.
- Physical characteristics of wetland systems control MeHg concentrations.

ARTICLE INFO

Article history:
Received 16 May 2012
Received in revised form 25 March 2013
Accepted 30 March 2013
Available online xxxx

Keywords:
Methyl mercury
DOM
Photodegradation
Photodemethylation
Optical properties
Fluorescence

ABSTRACT

Monomethyl mercury (MeHg) is a potent neurotoxin that threatens ecosystem viability and human health. In aquatic systems, the photolytic degradation of MeHg (photodemethylation) is an important component of the MeHg cycle. Dissolved organic matter (DOM) is also affected by exposure to solar radiation (light exposure) leading to changes in DOM composition that can affect its role in overall mercury (Hg) cycling. This study investigated changes in MeHg concentration, DOM concentration, and the optical signature of DOM caused by light exposure in a controlled field-based experiment using water samples collected from wetlands and rice fields. Filtered water from all sites showed a marked loss in MeHg concentration after light exposure. The rate of photodemethylation was 7.5×10^{-3} m^2 mol^{-1} (s.d. 3.5×10^{-3}) across all sites despite marked differences in DOM concentration and composition. Light exposure also caused changes in the optical signature of the DOM despite there being no change in DOM concentration, indicating specific structures within the DOM were affected by light exposure at different rates. MeHg concentrations were related to optical signatures of labile DOM whereas the percent loss of MeHg was related to optical signatures of less labile, humic DOM. Relationships between the loss of MeHg and specific areas of the DOM optical signature indicated that aromatic and quinoid structures within the DOM were the likely contributors to MeHg degradation, perhaps within the sphere of the Hg-DOM bond. Because MeHg photodegradation rates are relatively constant across freshwater habitats with natural Hg–DOM ratios, physical characteristics such as shading and hydrologic residence time largely determine the relative importance of photolytic processes on the MeHg budget in these mixed vegetated and open-water systems.

Published by Elsevier B.V.

1. Introduction

Mercury (Hg) contamination in wetland environments poses significant risks to humans and wildlife because wetland processes convert Hg to monomethyl mercury (MeHg), the form that is more readily concentrated in aquatic food webs (Mergler et al., 2007; Selin, 2009). In fish and wildlife, Hg accumulation has been associated with neurological and behavioral abnormalities, low reproductive success, and direct toxicity (Crump and Trudeau, 2009; Mitro et al., 2008; Wiener et al., 2003). These concerns have led to the listing of Hg as an important pollutant across the world and prompting United Nations Environment Programme (UNEP) international negotiations to address the Hg problem (http://www.chem.unep.ch/mercury/default.htm).

Wetlands are locations of MeHg production and subsequent transport to aquatic systems because they possess the optimal conditions for Hg methylation (Gilmour et al., 1992; St. Louis et al., 1996). Shallow flooded systems of all kinds, including rice agriculture

* Corresponding author. Tel.: +1 916 278 3063 (office); fax: +1 916 278 3071.
E-mail addresses: jafleck@usgs.gov (J.A. Fleck), gary.gill@pnnl.gov (G. Gill), bbergama@usgs.gov (B.A. Bergamaschi), tkraus@usgs.gov (T.E.C. Kraus), bdowning@usgs.gov (B.D. Downing), cnalpers@usgs.gov (C.N. Alpers).

0048-9697/$ – see front matter Published by Elsevier B.V.
http://dx.doi.org/10.1016/j.scitotenv.2013.03.107

and managed wetlands, also possess the optimal conditions for Hg methylation because of their repeated wet–dry cycles and available substrates for microbial activity (Hall et al., 2009; Windham-Myers et al., 2009). In California, shallow flooded habitats have been identified as responsible for a majority of in situ MeHg production in the Sacramento–San Joaquin Delta (Wood et al., 2010a,b). Rice agriculture constitutes a large proportion of the managed flooded lands in California, greater than the acreage of natural and managed non-agricultural wetlands throughout the state (Hill et al., 2006). Globally, rice production also contributes to a significant proportion of the wetland acreage in the lower Mississippi River watershed and much of southern and southeast Asia (USGS, 2000).

Because Hg is a global pollutant and locations where methylation occurs are widespread, it is important to understand the pathways for MeHg removal within aquatic systems to better protect human and ecosystem health (Sellers et al., 1996; Wiener et al., 2003). Photolytic degradation of MeHg, also referred to as photodemethylation, is an important component of the MeHg cycle (Hammerschmidt et al., 2006; Lehnherr et al., 2012; Li et al., 2010; Sellers et al., 2001). In coastal waters where chloride complexes predominate, OH radicals may play the primary role in MeHg degradation (Hammerschmidt and Fitzgerald, 2010). In freshwater systems, MeHg is more strongly associated with reduced organic functional groups within dissolved organic matter (DOM) that will increase photodegradation rates compared to coastal or ocean waters (Black et al., 2012; Zhang and Hsu-Kim, 2010). Other recent studies used isotopic methods to quantify the contribution of photodemethylation to the MeHg cycle in a number of systems (Bergquist and Blum, 2007; Kritee et al., 2012), but questions remain about the effects that DOM has on Hg-isotope fractionation (Zheng and Hintelmann, 2009, 2010). Despite recent studies focused on mechanisms, photodemethylation remains a poorly defined process in the natural environment.

DOM plays a complex role in both Hg cycling and photolytic reactions in aquatic systems. DOM strongly binds with the reactive inorganic form Hg^{II} (Han et al., 2006; Lamborg et al., 2003; Ravichandran, 2004) and MeHg (Hintelmann et al., 1997; Khwaja et al., 2010; Qian et al., 2002). Because of this DOM plays a role in the cycling and bioavailability of both Hg^{II} (Bergamaschi et al., 2012; Brigham et al., 2009; Choe et al., 2003; Dittman et al., 2010; Gorski et al., 2008; Gerbig et al., 2011; Graham et al., 2012; Schuster et al., 2011) and MeHg (Bergamaschi et al., 2011; Choe and Gill, 2003; Pickhardt and Fisher, 2007; Tsui and Finlay, 2011). DOM also binds with other radical-forming constituents that may participate in photochemical processes (Gu et al., 2011; Gao and Zepp, 1998). Specific components within DOM can release labile organic compounds and nutrients when exposed to light (Dalzell et al., 2009; Engelhaupt et al., 2003; Mopper and Kieber, 2000; Moran and Zepp, 1997). Additionally, photolytic reactions within the DOM can physically alter DOM structure by breaking large macromolecules into smaller components that are more available for bacterial utilization (Cory and McKnight, 2005; Blough and DelVecchio, 2002; Mostafa et al., 2007; Spencer et al., 2009). Alternatively, DOM that is dominated by fresh, low molecular weight structures can lead to the formation of larger DOM molecules and particles during light exposure, further complicating the effects of light exposure on DOM dynamics in natural systems (Stepanauskas et al., 2005).

Recent studies have reported contradictory lines of evidence regarding the role of DOM in photodemethylation. Zhang and Hsu-Kim (2010) implicated DOM binding in promoting photodemethylation. In contrast, Li et al. (2010) suggested that spatial trends in MeHg concentrations in waters from the Florida Everglades may have been related to DOM effectively shading the MeHg from solar radiation, thus maintaining higher MeHg concentrations where DOM was high. Meanwhile, Black et al. (2012) observed only a minor effect of DOM on demethylation rates.

Despite the recent contributions of these studies to our understanding of DOM effects on demethylation, none of the work was performed on unadulterated samples. Previous laboratory-based experiments used model compounds (i.e. glutathione (GSH)), commercially available isolates (Suwanee River Humic Acid (SRHA), International Humic Substances Society, St Paul, MN) and other forms of altered or synthesized DOM. The use of commercial standards, concentrated DOM, or isotope-labeled MeHg is useful in mechanistic studies but can significantly alter the DOM and its reactivity thus limiting the extrapolation of these studies to natural systems (Shubina et al., 2010). For instance, GSH is a good model compound for testing the effects of reduced sulfur groups in organic molecules in a well-constrained manner necessary for mechanistic studies, but it lacks the complexity of interactions within the structure of natural DOM to justify extrapolation to natural systems without corroborative field evidence. Isolates derived from natural DOM, like SRHA, are preferable to model compounds when making inferences about natural systems, but commercial isolates are also limited because they are known to have different properties than natural DOM due to the loss of important structural components in the isolation process (Shubina et al., 2010). Because DOM structure and reactivity is so complex, and dependent on conditions (ie. pH, ionic strength and DOM concentration), studies using natural water samples are necessary to bridge the gap between these valuable mechanistic lab studies and what occurs in natural systems.

Characterizing DOM sources and transformations in natural systems is important for improved understanding of biogeochemical processes, but such information is typically difficult or expensive to obtain. There are many ways to measure DOM properties, but most approaches require solid material, which requires large quantities of water and the isolation process typically alters the DOM and includes only a fraction of the bulk pool. One non-destructive method for the characterization of natural DOM that has received recent attention is optical characterization. The use of absorbance and fluorescence spectroscopy uses the inherent optical properties of DOM structures to infer the presence and relative distribution of organic structure and functional groups within the DOM. Furthermore, optical properties can be measured in situ at time-scales relevant to natural processes (Romera-Castillo et al., 2011). Recently, optical proxies have been used successfully to determine temporal variability in THg and MeHg concentration in dynamic hydrologic settings (Bergamaschi et al., 2011, 2012; Dittman et al., 2009).

In this study, we investigated changes in MeHg concentration and the relationship to changes in DOM and inherent optical properties of surface waters collected from rice fields and exposed to solar radiation in a controlled, field-based, bottle experiment. Our objective was to test whether in situ proxies for dynamic biogeochemical settings could be identified that would provide a way to observe MeHg dynamics in the field at timescales relevant to production and degradation processes. This information would be useful for improving our understanding of Hg cycling in natural systems and aid in making informed management decisions that minimize MeHg exposure both within these systems and in downstream habitats.

2. Methods

2.1. Field procedures

Water samples were collected from five field outlets within the Yolo Bypass Wildlife Area on the morning of July 30, 2008 (Table S1; Fig. S1A). Two were collected at the outlets of domestic (white) rice fields (R20, R66), two at the outlets of wild rice fields (W31, W64), and one was collected from a permanently flooded open-water wetland (PW5). All samples were collected early in the morning to minimize light exposure prior to the experiment. From each field location approximately 10 L of filtered surface water was collected in a polycarbonate carboy by pumping water through an acid-cleaned 0.45 μm filter cartridge using a peristaltic pump (Fig. S1C). The samples were filtered to

minimize biological activity within the samples during the experiment. The peristaltic pump was equipped with acid-cleaned C-flex pump head tubing and FEP Teflon® tubing on both the inlet and outlet. Ultra clean handling protocols were followed throughout equipment cleaning, sample collection, experimental manipulation, and analysis (Choe and Gill, 2003; Choe et al., 2003; Gill and Fitzgerald, 1985).

After rigorous mixing, each field sample was split into eleven 500 mL fluorinated ethylene propylene (FEP) Teflon® bottles (Fig. S1C). Six clear bottles were used for the "light" treatment and five opaque bottles were used for the "dark" treatment. The dark bottles were used as a control for possible changes not related to light exposure. For each wetland site, all sample bottles were placed in a 13 mm polypropylene mesh net and floated together on the surface of an open water pond to mimic the maximum potential natural exposure to ambient light at the water surface (Fig. S1D). Five time points (t0, t1, t2, t3, and t4) were sampled over a two-day period, representing a cumulative photon flux of 0, 20, 30, 50 and 80 mol m^{-2} of photosynthetically active radiation (PAR), respectively. Two bottles, one dark and one light, were not deployed, and these served as the time zero (t0) samples. At each successive time period, two bottles (one clear and one dark) were removed from each wetland site. Also, at each time point, one additional clear bottle was pulled from one of the wetlands to serve as a field replicate. Once collected, subsamples for DOM concentration and optical properties were poured from the clear bottles into an amber glass bottle and stored on ice until analysis. The remaining sample in each Teflon bottle was immediately preserved by acidification with high purity hydrochloric acid to 0.5% acid (v/v) and kept in the dark at room temperature until MeHg analysis. Whereas MeHg was analyzed at all time-points for both the clear and dark bottles, DOM subsamples were collected from only the dark bottles at the end of the experiment (t4) to serve as an experimental control.

Field measurements of ultraviolet (UV-A plus UV-B) and photosynthetically active radiation (PAR) were made continuously using a quantum sensor with nanologger (Apogee Instruments, Inc.) during the experiments to relate light exposure to MeHg and DOM degradation. The light sensor was located approximately 4 km from the location used for deployment of bottle incubations. Measurements are reported in moles of photons in the PAR wavelengths striking a square meter of water surface every second (mol m^{-2} s^{-1}). These were multiplied by the number of seconds for each PAR integration interval, giving an estimate of total light exposure, or cumulative PAR photon flux, in mol per square meter (mol m^{-2}). Although radiative energy in the UV wavelengths is primarily responsible for photolytic degradation of MeHg (Black et al., 2012; Lehnherr and St. Louis, 2009), the measurements of PAR correlated well with UV-A and UV-B energy measured at the site and with total radiation measurements at the nearby California Irrigation Management Information System (CIMIS) meteorological station in Davis, CA (http://wwwcimis.water.ca.gov/cimis/frontStationDetailInfo.do?stationId=6&src=info). Thus, PAR represents a surrogate for the relative amount of total light exposure in the experiment rather than assigning the mechanism to a single wavelength or wavelength range. Furthermore, the clear FEP Teflon® bottles used in this study are known to inhibit some of the radiative energy; however, they have been widely used in photodegradation studies because their high optical transparency requires only a small correction to obtain absolute degradation rates (Byington, 2007; Lehnherr and St. Louis, 2009). Caveats aside, the comparisons contained within this study were made across equivalent methodologies and exposure conditions and represent a general, yet meaningful, response of MeHg and DOM to light exposure in natural surface water environments.

2.2. Laboratory procedures

2.2.1. Monomethyl mercury analyses

Methylmercury analyses were performed at the Pacific Northwest National Laboratory Marine Sciences Laboratory, Sequim, WA. Concentrations were determined using distillation and aqueous phase ethylation followed by GC separation, pyrolysis and detection via cold vapor atomic fluorescence spectrometry (Bloom, 1989; Horvat et al., 1993). The accuracy and precision of the measurements were within 5% as indicated by an internal standard, laboratory replicates, and laboratory matrix spikes. The method detection limit for MeHg determinations was 0.012 ng L^{-1} based on three times the standard deviation (s.d.) of 7 replicate measurements of a low MeHg content aqueous sample. Absolute differences in 8 field replicate bottles within the experiment averaged 0.002 ng L^{-1} (s.d. 0.033 ng L^{-1}) which corresponded to a relative percent difference (RPD) of less than 3% for each site's field replicate except the lowest concentration site where the RPD was 15%.

2.2.2. Dissolved organic matter concentration

Measurements of DOM concentration and optical properties were performed at the U.S. Geological Survey (USGS) carbon research laboratory in Sacramento, CA on a carbon basis as DOC in mg C L^{-1} within 48 h of collection by high-temperature catalytic combustion using a Shimadzu TOC-V_{CNS} total organic carbon analyzer according to a modified version of method EPA 415.3 (U.S. Environmental Protection Agency, 2005). The accuracy and precision of the measurements were within 5% as indicated by an internal standard (caffeine), laboratory replicates, and matrix spikes. The long-term method detection limit for DOM concentration was 0.30 mg C L^{-1} based on three times the standard deviation of a low concentration standard measured over the annual cycle.

2.2.3. Optical characterization of DOM

Optical measurements of DOM are related to the light sensitive (chromophoric) portions of the DOM pool that absorb or fluoresce radiation in the ultraviolet and visible spectra. Spectral absorbance (A) was measured at 1 nm increments between 200 and 750 nm in a 0.01 m quartz cuvette using a CARY-300 spectrophotometer (Agilent Technologies, Santa Clara, CA, USA). Samples with A_{254} greater than 3 absorbance units (AU) were diluted and reanalyzed to ensure linearity of response in the wavelengths of interest. Absorbance values for wavelengths greater than 500 nm were below the level of reliable detection for a 1 cm cuvette so were removed from the analysis. Specific (carbon-normalized) absorbances for all wavelengths were calculated for concentration-independent comparisons of spectral shape across sites. The specific absorption at 254 nm has been related to the aromatic content of the DOM (Weishaar et al., 2003). Concentration-independent spectral slopes were also calculated for several wavelength ranges ($S_{275–295}$, $S_{290–350}$, $S_{350–450}$ and $S_{412–676}$, respectively) using a non-linear least-squares curve fitting technique for each specified spectral range (Boss and Zaneveld, 2003; Del Vecchio and Blough, 2002). Slope ratios were also calculated for the wavelength ranges within the ultraviolet spectrum (UV S_R: $S_{275–295}/S_{290–350}$) and the ultraviolet to visible spectra (UV–vis S_R: $S_{275–295}/S_{412–676}$). Spectral slopes and slope ratios were calculated using MatLab R2008a (MathWorks, Natick, Massachusetts, USA) to infer DOM composition with higher slope values indicating a low molecular weight or "fresh" microbial or algal contribution to DOM and slope ratios further indicating the relative molecular size (Helms et al., 2008). The accuracy and precision of the measurements were within 5% as indicated by an internal standard (potassium dichromate) measured monthly, a laboratory reference material (Lipton® unsweetened iced tea, 1% by volume) measured daily, and laboratory replicates measured approximately every 10 samples. The long-term method detection limits vary by wavelength, ranging from 0.001 AU at 650 nm to 0.008 AU at 250 nm based on three times the standard deviation of field method blanks over the annual cycle.

Fluorescence was measured using a SPEX Fluoromax-4 spectrofluorometer equipped with a 150 W Xenon lamp (Horiba Jobin Yvon, NJ,

USA). Fluorescence intensity was measured at excitation wavelengths (ex) of 200 nm to 440 nm at 10 nm increments and emission wavelengths (em) of 300 nm to 600 nm at 5 nm increments on room temperature samples (25 °C) in a 0.01 m quartz cell. Instrument corrections were applied and results were water Raman-normalized. Concentration-related inner filter effects were corrected using wavelength and slit-width dependent corrections as described by Gu and Kenny (2009). Fluorescence results are shown as contour plots of fluorescence intensities in Raman-normalized fluorescence units (RFU) across the excitation and emission spectra creating a 3 dimensional excitation–emission matrix (EEM) for each sample (Cory et al., 2011). Individual diagnostic peaks within the EEMs spectra (Table 1) were identified according to previous efforts (Coble, 1996, 1990, 1998; Stedmon et al., 2003) with the addition of two peaks: 1) "FDOM" at excitation 370 and emission 460 (ex370em460) corresponding to field instrumentation (Bergamaschi et al., 2011; Downing et al., 2009) and 2) a previously unidentified area "peak Z" (ex420em460) that represented a baseline for humic-like fluorescence. The accuracy and precision of the measurements were within 5% as indicated by an internal standard (quinine sulfate) measured quarterly, a laboratory reference material (Lipton® unsweetened iced tea, 1% by volume) measured daily, and laboratory replicates measured approximately every 10 samples. The long-term method detection limits vary by excitation-emission pairs, ranging from 0.001 RFU throughout much of the EEM spectra to 0.354 RFU in the region of the peak B based on three times the standard deviation of field method blanks over the annual cycle. Fluorescence spectra were also analyzed using parallel factor analysis, or PARAFAC, to identify the important EEM pairs in the EEM spectra across all samples (Stedmon et al., 2003).

Changes in DOM composition were evaluated using published derivations of fluorescence properties (Table 1). For comparison of fluorescence EEM shape across sites with differing concentrations, carbon-normalized EEM plots were also calculated by dividing the fluorescence intensities by DOM concentration across the entire EEM spectra, hereafter referred to as C-normalized fluorescence. Three published fluorescent DOM compositional indicators were also calculated. Fluorescence index (FI) was calculated as the ratio of emissions 470 nm and 520 nm at excitation 370 nm for corrected spectra according to Cory et al. (2010) as an indicator of relative microbial versus terrestrial contributions to the chromophoric DOM pool. Humic Index (HIX) was calculated as an indicator of source, diagenesis and sorptive capacity (Ohno, 2002; Ohno et al., 2008). The freshness index (β:α), an indicator of the contribution of recently produced DOM, was measured as the ratio of emission intensity at 380 nm divided by the maximum emission intensity between 420 and 435 nm at excitation 310 nm with higher values representing a higher proportion of fresh DOM (Parlanti et al., 2000; Wilson and Xenopoulos, 2009). Finally, the optical ratio of fluorescence (ex370 em460) to absorbance at 370 nm, known as the relative fluorescence efficiency (RFE), was calculated as an indicator of the relative amount of algal and non-algal DOM (Downing et al., 2009).

2.3. Data analyses

Graphical and basic statistical analyses were performed in both Excel 2003 and Sigmaplot® (version 11, Systat Software, Inc., San Jose, Calif.). Analyses of variance (ANOVAs) were performed on the calculated MeHg degradation rates for each time point of the experiment using a one-way ANOVA test followed by the Holm–Sidak multiple pairwise comparison method to determine significance of differences between sites. To examine which part of the absorbance and fluorescence spectra were most strongly related to MeHg concentration and percent MeHg loss, we calculated the correlation coefficients between MeHg concentration and percent loss and each individual absorbance wavelength and fluorescence wavelength pair over the course of the light exposure incubation. This graphical approach has been used to identify regions within optical spectra related to reactivity of DOM and the production of disinfection byproducts (Kraus et al., 2010). Correlation coefficients (R) were calculated using the Pearson Product Moment function in Excel and confirmed with Sigmaplot® (v.11).

Exploratory data analyses were performed using The Unscrambler® X version 10.1 (CAMO Software, Oslo, NORWAY) on both concentration and percent change data. Principle component analyses (PCA) were performed using Non-linear Iterative Partial Least Squares of mean-centered, untransformed and data with cross validation. Because PCA allowed the simultaneous inclusion of both DOC and optical variables, all optical measurements in the PCA were carbon-normalized to focus on the relative difference in spectral shape rather than having redundant concentration effects.

3. Results and discussion

3.1. Initial conditions

The samples collected in this study had a wide range of MeHg and DOM concentrations, and DOM character (Table 1). Although DOM concentrations were higher than previous studies in lakes and wetland-derived waters, the $SUVA_{254}$ values were lower and absorption slopes (S) were higher than the DOM in those studies reflecting a smaller, relatively low aromatic content of the DOM within this study (cf. Helms et al., 2008; Weishaar et al., 2003). In general, water from two fields had similar absorbance signatures (domestic rice field R20 and wild rice field W31), and the three other fields had unique absorbance spectra (R66, W64, and PW5) providing four distinct absorbance signatures for the experiment (Table 1). Site W64 had the lowest $SUVA_{254}$ (1.24 versus 2.4 to 2.5 L mg^{-1} cm^{-1}) and highest S and S_R values. The unique absorbance in W64 was likely related to high algal production observed during this study (data not shown). Site PW5 also had elevated S and S_R values relative to W31, R20 and R66 but not as elevated as W64. Site R66 had generally lower S values than W31 and R20 but similar S_R values which may indicate a similar source of DOM as R20 and W31 but different molecular size.

Initial (t0) carbon-normalized EEM spectra were relatively similar across sites and were dominated by humic-like fluorescence in the regions referred to as peak A and peak C which are common components in DOM spectra (Table 1; Stedmon et al., 2003). Although less pronounced and more variable, there were fluorescence signatures in the EEMs regions known as peaks N, T and B in some of the samples (Coble et al., 1998; Stedmon et al., 2003). Peak N has been associated with algal productivity (Coble et al., 1998) whereas peaks T and B have been associated with protein-like structures and lignin degradation products (Baker and Spencer, 2004; Hernes et al., 2009; Stedmon et al., 2003). One sample (W64) had generally lower carbon-normalized fluorescence intensities across the EEM spectra matrix compared to the other sites. Mentioned earlier, this site had the most algal production which may have contributed large amounts of non-chromophoric DOM thus decreasing the relative fluorescence across the spectra.

The humic index (HIX) and fluorescence index (FI) values were in the ranges 0.80 to 0.90 and 1.47 to 1.59, respectively. These values indicate DOM was largely terrestrial in origin with minor differences in the contribution of microbial DOM (McKnight et al., 2001; Ohno, 2002). All samples had similar HIX values around 0.9 except W64 (0.8); whereas, FI values were similar across all samples except PW5 (Table 1). The sample from PW5 was uniquely high in relative fluorescence efficiency. This may indicate a larger microbial contribution to the DOM signature for the PW5 site. In general, there were three fields with similar DOM optical signatures (R20, R66, and W31) and two other fields with unique DOM signatures (W64 and PW5) indicating three distinct fluorescence starting conditions (Table 1).

Table 1
Comparison of methylmercury and diagnostic dissolved organic matter measurements between sites for initial conditions (t0) prior to the light exposure incubation experiment. The sites are identified by their field number in the wetland complex preceded by the type of field management where "R" represents domesticated (white) rice, "W" represents wild rice, and "PW" represents permanent wetland pond (see Table S1).

Measurement	Name (units)	Property/purpose	Reference	R20	R66	W31	W64	PW5
1a. Concentration-based measurements								
Dissolved (<0.45 μm filter-passing) monomethyl mercury	f-MeHg (ngHg L^{-1})	Concentrations used to calculate photodemethylation rates	Horvat et al., 1993	1.50	0.50	0.70	3.75	0.18
Dissolved organic carbon	DOC (mg C L^{-1})	Dissolved organic matter concentration on a carbon-basis	U.S. EPA method 415.3	13.8	8.5	16.8	36.3	10.2
Ratio of MeHg to DOC	MeHg/DOC (ng Hg mg C^{-1})	Related to binding site strength and availability	Haitzer et al. (2002)	0.11	0.06	0.04	0.10	0.02
Total dissolved nitrogen concentration	TDN (mg L^{-1})	Total dissolved nitrogen concentration	Merriam et al. (1996)	1.34	0.81	1.75	5.92	0.93
Absorbance intensity at 350 nm	A_{350} (AU cm^{-1})	General absorbance of DOM, related to general carbon bonding	Baker and Spencer (2004)	0.07	0.05	0.09	0.11	0.04
Absorbance intensity at 440 nm	A_{440} (AU cm^{-1})	General absorbance of DOM, related to algal activity in some cases	Hulatt et al. (2009); Zhao et al. (2009)	0.01	0.01	0.02	0.03	0.01
1b. Absorbance-based DOM character measurements								
Specific ultraviolet absorbance at 245 nm	$SUVA_{254}$ (L mg^{-1} m^{-1})	Relative aromatic content of DOM	Weishaar et al. (2003)	2.41	2.58	2.41	1.50	2.22
Spectral slope between 275 and 295 nm	$S_{275–295}$	Relative molecular weight/size of DOM	Helms et al. (2008)	0.0179	0.0160	0.0179	0.0196	0.0198
Spectral slope between 290 and 350 nm	$S_{290–350}$	DOM composition	Blough and DelVecchio (2002)	0.0175	0.0156	0.0173	0.0176	0.0188
Spectral slope between 350 and 400 nm	$S_{350–400}$	Relative molecular weight/size of DOM	Helms et al. (2008)	0.0179	0.0160	0.0182	0.0140	0.0178
Spectral slope between 412 and 676 nm	$S_{412–676}$	DOM composition, photobleaching	Twardowski et al. (2004)	0.0164	0.0156	0.0150	0.0116	0.0171
Ratio of spectral slopes in the ultraviolet spectrum	UV S_R	Relative molecular weight/size of DOM	Helms et al. (2008)	0.98	0.97	0.95	1.26	1.06
Ratio of spectral slope in the ultraviolet range to the spectral slope in the visible range	UV–vis S_R	DOM source, degree of photolytic alteration	This study	1.09	1.03	1.20	1.68	1.16
1c. Fluorescence-based DOM character measurements (carbon-normalized, value/DOC × 100)								
Carbon-normalized fluorescence intensity at ex260em450	peak A (RFU, c-norm)	Relative amount of "humic-like" DOM	Coble, 1996 (1990); Stedmon et al. (2003)	16.1	18.7	17.9	9.8	17.7
Carbon-normalized fluorescence intensity at ex270em305	peak B (RFU, c-norm)	Relative amount of "protein-like" DOM	Coble (1996, 1990); Stedmon et al. (2003)	1.6	3.2	1.7	2.9	3.0
Carbon-normalized fluorescence intensity at ex340em440	peak C (RFU, c-norm)	Relative amount of "humic-like" DOM	Coble (1996, 1990); Stedmon et al. (2003)	8.0	10.2	8.9	4.5	8.1
Carbon-normalized fluorescence intensity at ex390em510	peak D (RFU, c-norm)	Relative amount of soil "fulvic-like" DOM	Coble (1996, 1990); Stedmon et al. (2003)	3.4	4.3	3.9	2.0	3.5
Carbon-normalized fluorescence intensity at ex300em390	peak M (RFU, c-norm)	Relative amount of "marine-like" DOM	Coble (1996, 1990); Stedmon et al. (2003)	7.9	9.6	8.8	5.0	8.0
Carbon-normalized fluorescence intensity at ex280em370	peak N (RFU, c-norm)	Relative amount of algal derived DOM	Coble et al. (1998)	6.0	7.5	6.9	5.0	6.6
Carbon-normalized fluorescence intensity at ex270em340	peak T (RFU, c-norm)	Relative amount of "protein-like" DOM	Coble (1996, 1990); Stedmon et al. (2003)	3.3	5.0	3.8	4.2	4.1
Carbon-normalized fluorescence intensity at ex370em460	FDOM (RFU, c-norm)	Relative amount of "quinoid-like" humic DOM, in situ cdom fluorescence probe window	Downing et al. (2009)	5.9	7.6	6.8	3.5	6.8
Carbon-normalized fluorescence intensity at ex420em460	peak Z (RFU, c-norm)	Baseline DOM fluorescence	This study	1.5	2.0	1.8	0.9	1.5
Humification index	HIX	Relative measurement of sorption capacity; C:O and C:N, carboxyl content	Ohno (2002)	0.90	0.87	0.89	0.81	0.87
Fluorescence index ex370em520/ex370em480	FI	Relative contribution of terrestrial and microbial sources to the DOM pool	Cory et al. (2010)	1.47	1.50	1.49	1.48	1.59
Freshness index	β:α	Relative contribution of fresh DOM to recalcitrant DOM	Parlanti et al. (2000); Wilson and Xenopoulos (2009)	0.75	0.76	0.78	0.86	0.81
Relative fluorescence efficiency (FDOM/A370)	RFE (RFU/AU)	Microbial (non-algal) to algal ratio	Downing et al. (2009)	15.8	15.4	17.4	13.2	22.1

3.2. Photolytic degradation of MeHg

Methylmercury concentrations in clear bottles decreased with increasing exposure to solar radiation at rates independent of initial concentration. Both MeHg loss in the clear bottles at each time point relative to the initial concentration ($[MeHg]_t/[MeHg]_0$), and the MeHg loss in clear bottles relative to the dark bottles at the same time point ($[MeHg]_{t,clear}/[MeHg]_{t,dark}$), showed similar trends (Fig. 1). Linear and exponential regressions provided strong fits of the data, although the regressions for $[MeHg]_t/[MeHg]_0$ were stronger than $[MeHg]_{t,clear}/[MeHg]_{t,dark}$ ($r^2 = 0.87$ and 0.88 versus $r^2 = 0.51$ and 0.52, respectively). The regression equation slopes represent the loss rate of MeHg as a rate constant (k_{pd}) dependent on cumulative PAR exposure and initial MeHg concentration. The linear

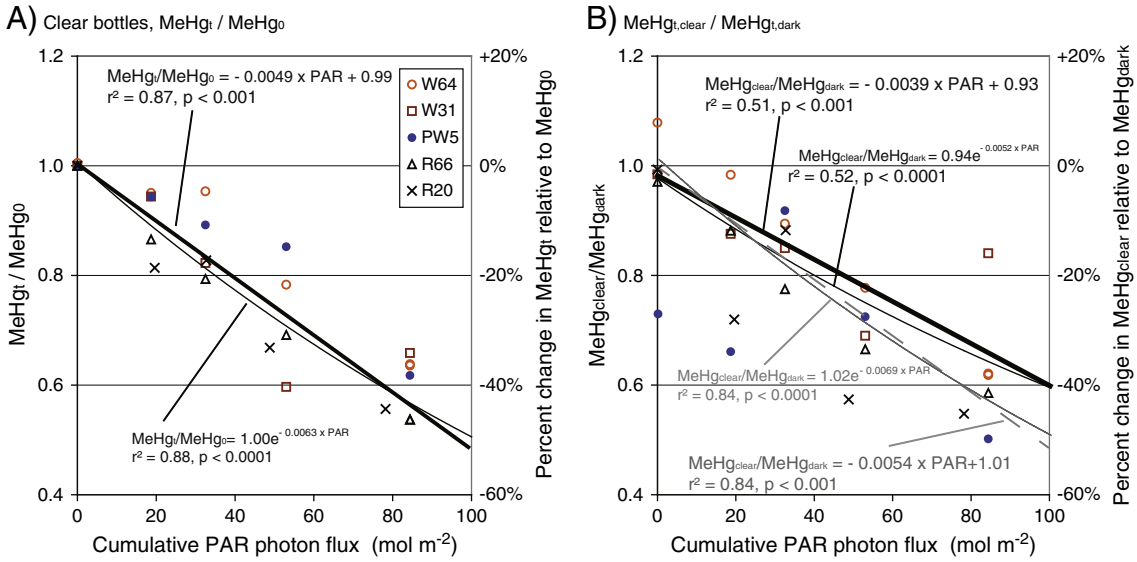

Fig. 1. Changes in MeHg concentration as a result of light exposure. Figure A shows the change in MeHg concentration plotted against cumulative photosynthetic available radiation (PAR) for clear bottles at each time point relative to the initial (t0) sample from that location. Figure B shows the ratio of MeHg concentration in clear bottles to their paired dark bottles at each time point in the experiment. Linear and exponential regressions are shown on both plots. The dashed line in Figure B shows the linear regression when four outliers were removed from the analysis.

regression slopes suggest a k_{pd} of approximately 0.005 m^2 mol^{-1} (Fig. 1); however, it is important to note that the k_{pd} for MeHg was calculated over a time period of light exposure in which the loss appeared to be linear (cumulative PAR of 80 mol m^{-2}). Because other work that measured loss over a greater PAR exposure (180 to 320 mol m^{-2}) used the rate loss equation (Eq. (1)), and the exponential regression fits for the PAR exposure in this study were slightly better than the linear fits, we chose to report k_{pd} using the same first-order rate loss equation similar to others so that we could better extrapolate the results of this study to systems with greater PAR exposure conditions (Lehnherr and St. Louis, 2009; Li et al., 2010).

$$\ln[\mathrm{MeHg}]t = \ln[\mathrm{MeHg}]0 - (\mathrm{kpd} \times \text{Cumulative PAR photon flux}). \quad (1)$$

Using Eq. (1), we calculated the rate constants (k_{pd}) for each time point in the experiment to determine if any changes in the rate occurred throughout the light exposure period. Rate constants for the clear bottles ranged from 0.0043 to 0.0081 m^2 mol^{-1}, whereas the rate constants for the dark bottles ranged from −0.0017 to 0.0016 m^2 mol^{-1} (Table S2). All k_{pd} for clear bottles were significantly greater than their respective dark bottle pair ($p < 0.05$; Holm–Sidak post-hoc test). When dark bottle rates were subtracted from clear bottles to isolate changes due to the effects of light exposure alone, there were no differences between k_{pd} across sites ($p < 0.05$; Holm–Sidak post-hoc test). The median k_{pd} for the "clear-dark bottle treatment" was 0.0063 m^2 mol^{-1} (s.d. = 0.0030), which is identical to the k_{pd} from the exponential regression for $[\mathrm{MeHg}]_t/[\mathrm{MeHg}]_0$ (0.0063 m^2 mol^{-1}). When correcting for Teflon interference, the median rate constant (k_{pd}) for all clear bottles was 0.0075 m^2 mol^{-1} in this study, well within the range of 0.006 to 0.015 m^2 mol^{-1} reported by Black et al. (2012) for nearby wetland-derived water mixtures and other natural and experimental waters across North America (Table 2).

The degradation rate of MeHg did not differ between samples despite differences in DOM concentration and character. The differences in k_{pd} across the DOM range were even less than those reported in experimental water mixtures prepared from nearby wetlands (Table 2). This result is consistent with the predominance of strong binding

Table 2
Summary of photodemethylation rates reported for sites across North America.

$k_{pd} \times 10^{-3}$	$k_{pd} \times 10^{-3}$ corrected[2]	Location	Water source	MeHg source	MeHg (ng L^{-1})	DOM (mgC L^{-1})	Reference
4–10	5.2–13	ELA, Ontario, Canada	Lake	Native	1.1	17	Sellers et al. (1996)[1]
2–4	2.6–5.2	ELA, Ontario, Canada	Lake	CH_3HgCl spike	4.5–6	17	Sellers et al. (1996)[1]
3.82	4.5	ELA, Ontario, Canada	Lake	$CH_3^{199}Hg$ spike	1.2	12.8	Lehnherr and St. Louis (2009)
3.93	4.5	ELA, Ontario, Canada	Lake	Native	0.8	12.8	Lehnherr and St. Louis (2009)
8	10	Marcell, Minnesota, USA	Lake	CH_3HgCl spike	8.3	11	Hines and Brezonik (2004)[1]
10.87	13.67	Everglades, Florida, USA	Freshwater wetland	$CH_3^{201}Hg$ spike	0.6	6–22	Li et al., 2010
–	–	Laboratory experiments	Commercial isolate, model compounds	CH_3HgCl spike	>100	0–2	Zhang and Hsu-Kim (2010)
3.0	3.8	Alaska, USA	Lake	CH_3HgCl spike	1.2–4.2	0.4–10	Hammerschmidt and Fitzgerald (2010)[1]
–	9.9 +/− 2.0	San Francisco, CA, USA	Coastal wetland	CH_3HgCl spike	0.02–1.25	1.5–11.3	Black et al. (2012)
–	3.2 +/− 1.0	San Francisco, CA, USA	Coastal ocean	CH_3HgCl spike	0.02–1.25	1.5–11.3	Black et al. (2012)
6.3 +/− 3.0	7.5 +/− 3.5	Sacramento, CA, USA	Freshwater wetland, rice field	Native	0.2–3.8	8.5–36.3	This study

[1] k_{pd} are estimated from calculations using data from tables or charts and/or local daily PAR during the study.
[2] Corrections range from 1.2 to 1.35 based on type of Teflon bottle used.

Please cite this article as: Fleck JA, et al, Concurrent photolytic degradation of aqueous methylmercury and dissolved organic matter, Sci Total Environ (2013), http://dx.doi.org/10.1016/j.scitotenv.2013.03.107

between Hg and DOM at reduced sulfur groups at environmentally relevant concentrations of Hg (<1 μg Hg mg C^{-1}; Haizer et al., 2002; Ravichandran, 2004). Although DOM alters MeHg photosensitivity because of the effects that the thiol binding between DOM and MeHg has on the Hg–C bond in the MeHg molecule (Zhang and Hsu-Kim, 2010), Hg and MeHg binding occurs at a small fraction of the DOM sites where thiol complexes occur thus minimizing any effect DOM composition may have on MeHg photolytic degradation. The exception to this scenario is the rare condition where aqueous Hg concentrations are elevated to the degree that the strong thiol binding site capacity of the DOM is exceeded (Haitzer et al., 2002; Zhang and Hsu-Kim, 2010), or the less rare condition where the actinic flux is significantly reduced in the water column by DOM absorbance effectively shading the MeHg from radiation in deeper water strata (Li et al., 2010). Neither condition was met under the conditions of this study.

3.3. Photolytic degradation of DOM

3.3.1. Effect of light exposure on DOM concentration

The concentration of DOM measured on a carbon basis did not change significantly with light exposure. Concentrations changed by less than 7% in all clear bottles over the entire exposure period, and percent loss did not differ significantly from dark control bottles ($t = -1.53$, $p = 0.165$, $df = 8$). Bulk concentrations of DOM rarely change significantly over short periods of light exposure because the photosensitive DOM portion usually comprises a small fraction (1 to 5%) of the total DOM pool. However, changes in DOM composition (structural alterations) may occur within the bulk DOM pool without affecting bulk DOM concentrations (Cory et al., 2011; Spencer et al., 2007).

3.3.2. Effect of light exposure on DOM absorbance

Although bulk DOM concentrations did not change significantly as a result of light exposure, changes in the absorbance spectra indicated changes in the light sensitive (chromophoric) structures within the DOM (Fig. S2; Table S3). In general, light exposure caused a decrease in the total amount of light absorbed across the full absorbance spectrum with maximum losses occurring in the wavelengths between 330 nm and 450 nm (Fig. S2B–D). Many DOM structures absorb light in this region including aromatic compounds, lignin degradation products, pigments, and other organic structures derived from the decay of terrestrial and emergent wetland plants (Del Vecchio and Blough, 2004; Hernes et al., 2009; Minor et al., 2007) and algal sources (Hulatt et al., 2009; Zhang et al., 2009).

Although DOM from all sites showed loss of absorbance between 330 and 450 nm, there was a difference in loss patterns between management types. DOM from the white rice fields (R20 and R66) showed similar patterns in the loss of absorbance with maximum losses occurring at all wavelengths of >350 nm (Fig. S3A, D). In contrast, DOM from the wild rice fields (W31 and W64) showed a similar maximum percent loss in absorbance near 350 nm but the loss diminished between 350 and 450 nm (Fig. S3B, C). The DOM from field W64 showed unique changes at wavelengths of >350 nm as the light exposure experiment continued. The relative standard deviation in absorbance for field W64 showed a strong inflection point for relative changes in absorbance at 440 nm (Fig. S2B), an area of DOM absorbance known to be related to algal activity. Field W64 possessed higher chlorophyll (data not shown) and may have had a wider distribution of algae and a more complex assemblage of pigments which could explain the unique absorbance spectral response to light exposure. The sample from field W64 may have even contained nanoplanktonic particles that were small enough to have passed through the filter and continued to be active throughout the experiment. Evidence of this possibility resides in the fact that the large increase in W64 absorbance at wavelengths over 400 nm was exaggerated by the spectral correction for scattering in which the absorbance in the range of 700 to 750 nm is used to calculate spectral slopes and the degree of increase was not observed in the raw spectra (Table 1). Alternatively, the higher contribution of DOM from algae or plankton in the sample from field W64 may have led to condensation reactions that caused the formation of colloids or large DOM structures that absorb in the visible wavelengths (Kieber et al., 1997; Stepanauskas et al., 2005).

Changes in the spectral slopes of the absorbance curve caused by light exposure indicated structural changes in the DOM related to molecular size and origin. The ultraviolet slope ratio ($S_{275-290}/S_{350-400}$) increased with light exposure by as much as 15%, suggesting that photolytic degradation decreased the average molecular size of the DOM in most cases (Helms et al., 2008). The large structures proposed to have formed in W64 sample were not captured in the absorption slope data because the slopes calculated in this study did not cover the range of absorbance caused by these structures (Downing et al., 2009). Future research efforts should consider extending the slope calculations into longer wavelengths to capture possible condensation products.

3.3.3. Effect of light exposure on DOM fluorescence

Carbon-normalized fluorescence intensities decreased across the EEMs spectra following light exposure (Fig. 2). By comparing carbon-normalized EEMs spectra in the clear bottles prior to light exposure (t0) with the spectra after the full period of light exposure (t4) the areas where the greatest change in the spectra occurred is apparent (Fig. 2, Table S3). A comparison between the EEMs spectra of the clear bottles and dark bottles at t4 showed a similar trend whereas a comparison between the t0 samples and dark bottles at t4 showed little change, indicating that the changes were caused by photolytic processes (Fig. S4). The greatest percent loss in fluorescence intensity occurred in the region centered near excitation 370 and emission 400 nm (ex370 em400) for all samples (Fig. 2; Fig. S5). This EEMs region has not received much attention regarding studies linking structural information with fluorescence spectra, but the region falls near the edges of the regions typically associated with terrestrially derived humic acids (ex370, em420–480; Coble, 1996; Cory et al., 2011; Stedmon et al., 2003) and fulvic-like DOM derived from green algae (ex320–340, em400–450; Nguyen et al., 2005). More directly, this area falls at the lower edge of the region measured by in situ sensors (ex370 em400–460) in studies linking fluorescence and MeHg (Bergamaschi et al., 2011). In addition, there was a measurable increase in the region of peak B (ex280 em305) following light exposure in some cases. This region is typically associated with "protein-like" fluorescence (Baker and Spencer, 2004; Stedmon et al., 2003), but it also encompasses other refractory structures such as tannic phenols which complicates interpretation of structural relationships in this area of the EEMs (Hernes et al., 2009; Mostafa et al., 2007).

The fluorescence ratios used to identify DOM composition in previous studies changed little as a result of light exposure, at least for the period of exposure in this study (Table S3). The humic index (HIX) decreased with increasing light exposure for all samples but only by a small fraction. The fluorescence index (FI), used to assess the relative amount of terrestrial and microbial DOM in the bulk pool (Cory et al., 2010; McKnight et al., 2001), changed less than 2% with light exposure. The freshness index (β:α) changed even less with light exposure. Only the lesser-known calculated indicator known as the relative fluorescence efficiency (RFE), which is calculated from both absorbance and fluorescence data, changed markedly with light exposure in this study.

The lack of significant change in the fluorescence indicators suggests that, while these indicators may be sensitive to differences in DOM source and microbial alteration, they are minimally affected by changes due to abiotic processes, like solar radiation. That is not to

ARTICLE IN PRESS

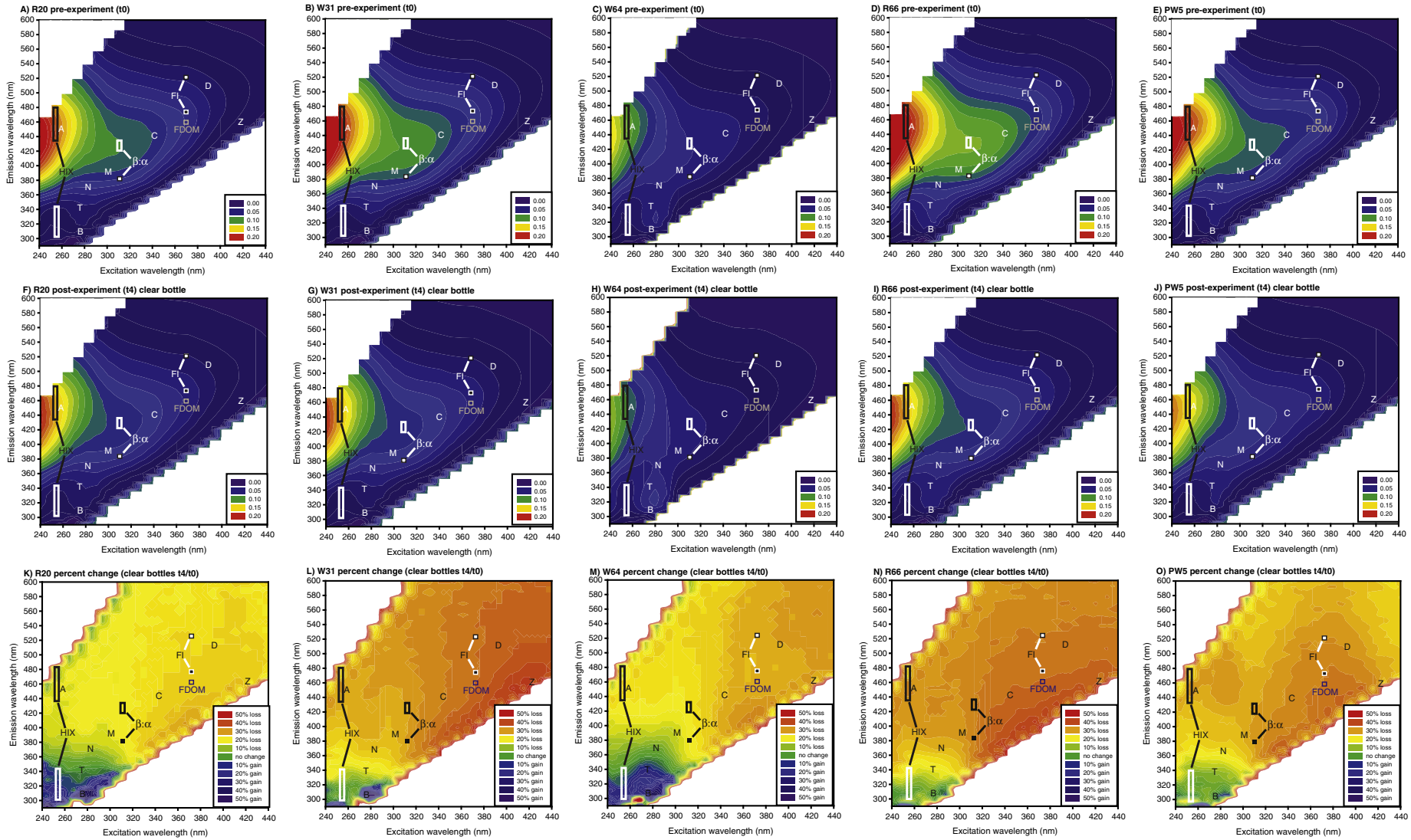

Fig. 2. Changes in carbon-normalized, excitation-emission matrix (EEM) fluorescence intensity spectra as a result of light exposure. Figures A through E show EEMs for clear bottles prior to light exposure (t0). Figures F through J show EEMs for clear bottles after the full period of light exposure (t4). Figures K through O show the percent change in fluorescence intensity across the EEMs in the clear bottles relative to t0 (I/I_0). In figures A though J, yellow to orange shades indicate higher fluorescence intensities. In figures K through T, orange and yellow shades indicate a decrease in fluorescence, blue shades indicate an increase in fluorescence, and green shades indicate minimal changes. Named peaks (Coble, 1996; Stedmon et al., 2003) and areas used for calculating indicators (Cory et al., 2010; Ohno, 2002) are labeled.

Please cite this article as: Fleck JA, et al, Concurrent photolytic degradation of aqueous methylmercury and dissolved organic matter, Sci Total Environ (2013), http://dx.doi.org/10.1016/j.scitotenv.2013.03.107

say the fluorescent DOM is not affected in these regions but that the regions are affected similarly such that the ratios do not change. For instance, the areas of the EEMs used to calculate the FI decreased to a similar degree during light exposure which resulted in little change in the FI ratio (Table S3; Fig. 2). This was true for the β:α ratio as well (Table S3). The lack of change in both FI and β:α reaffirms their use as indicators of microbial DOM and provides evidence that there was minimal microbial activity during incubation within this study. It is likely that the HIX did not change more because samples that are already predominantly humic are insensitive to losses in the non-humic region. Ratios of fluorescence to absorbance are better at discriminating between photodegradation and microbial processing of DOM than fluorescence or absorbance alone which may explain the changes in RFE seen in this study (Romera-Castillo et al., 2011).

It is worth noting that photolytic degradation led to a more uniform fluorescence signature across sites (Fig. 3, Fig. S6). The trend toward uniformity following light exposure may represent a base refractory pool of chromophoric DOM across the sites in this study. This was seen more clearly by comparing the relative standard deviation (RSD) in C-normalized EEMs across the sites prior to and after light exposure (Fig. 3). The difference in the EEMs across sites was high for bottles not exposed to light (t0, dark bottle t4) and showed specific areas of greater variance in the peak A and peak C regions (Fig. 3A) whereas the same samples exposed to light (clear bottle at t4) were more similar in EEMs spectra across sites (Fig. 3B). The difference between the relative standard deviation (RSD) for samples that were exposed to light (clear bottles t4) and those that were not exposed to light (t0, dark bottle t4) indicated that the greatest relative changes in carbon-normalized fluorescence between sites occurred in a band of wavelengths in the "Type IV" region of the EEMs including a marked decrease around peak N, an area previously attributed to DOM of phytoplankton origin and an increase in the area between peak B and peak T attributed to proteins containing ring structures and phenolic degradation products (Chen et al., 2003; Coble et al., 1998; Stedmon et al., 2003).

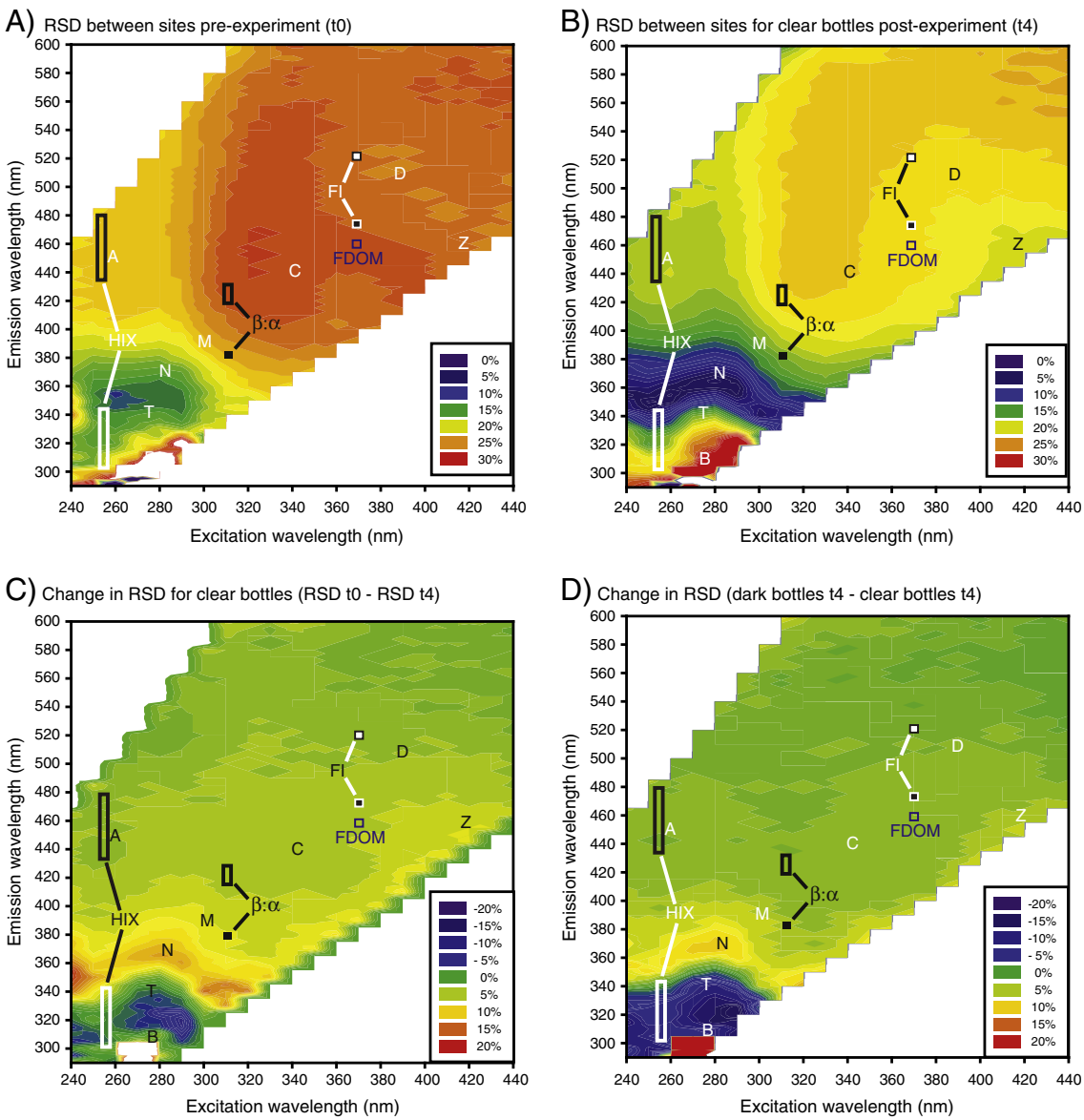

Fig. 3. Differences in fluorescence signatures between sites measured as the relative standard deviation (RSD) of carbon-normalized fluorescence intensities across the fluorescence spectra across all sites. Figure A shows the RSD across all sites prior to light exposure (t0). Figure B shows the RSD across all sites after light exposure in the clear bottles (t4). Figure C shows the difference between RSD at t0 and t4 in the clear bottles. Figure D shows the difference between the dark and clear bottles at t4. Figures C and D highlight the areas of the fluorescence signature that changed most across sites as a result of light exposure. The area of the spectra below the "B" peak has a large RSD because of large analytical error and not changes in measureable fluorescence. Absolute standard deviations and the RSD plots for the dark bottles are shown in Fig. S6.

Please cite this article as: Fleck JA, et al, Concurrent photolytic degradation of aqueous methylmercury and dissolved organic matter, Sci Total Environ (2013), http://dx.doi.org/10.1016/j.scitotenv.2013.03.107

Parallel factor analysis (PARAFAC) verified the identification of the areas of the EEMs where differences occurred. For this study, a four component PARAFAC model captured a majority of the variance in the EEMs spectra across sites and light exposure (Fig. S7A–D). Component 1 was in the area of peak A (ex < 280 em > 440) with a secondary component in the area of peak D (Stedmon et al., 2003). Component 2 was in the area of peak M and peak N (Coble, 1996; Coble et al., 1998). Component 3 was distinctly similar to the tryptophan-like peak T of bacterial or algal origin (Cory and McKnight, 2005; Stedmon et al., 2003). Component 4 was also distinctly in the humic region of peak C (Coble, 1996; Stedmon et al., 2003). In general, the components were similar to a subset of those identified by C-normalized EEMs intensity and difference plots (Fig. 2). Within the PARAFAC model, components 1 and 2 changed little over the time series of light exposure (Fig. S7E). In contrast, component 3 (protein-like) increased while component 4 (humic-like) decreased with increasing light exposure (Fig. S7E). This analysis corroborates the previous analysis that suggested photolytic degradation of DOM was focused in aromatic regions of the DOM. The use of the PARAFAC model in this analysis does not identify the total loss of fluorescence but rather is related to the relative changes in the EEMs spectra across sites and exposure. The small dataset for which PARAFAC could be performed would not allow for discrimination of EEMs differences between sites and light exposure independently, limiting our ability to elucidate between changes due to photodegradation within sites and differences in DOM between sites.

3.4. MeHg–DOM relationships

Although there was not an apparent relationship between DOM concentration and demethylation rate, the role of DOM in photolytic processes is complex and may still play a major role in MeHg degradation by mediating radical formation or transferring its energy to the Hg–C bond (Black et al., 2012; Blough, 2001). More information about DOM and its degradation may provide insights to the possible photodemethylation pathways and help narrow whether production of singlet oxygen ($^1O_2$) or hydroxyl radicals (OH•) in bulk water dominate demethylation (Hammerschmidt and Fitzgerald, 2010; Zhang and Hsu-Kim, 2010) or internal production of radicals within the sphere of influence of aromatic DOM (Latch and McNeil, 2006) further contribute to the complex role DOM plays in demethylation (Black et al., 2012).

The relationship between MeHg concentration and individual absorbance intensities was strongly positive across the entire range of wavelengths from 200 to 500 nm ($R > 0.85$, $p < 0.001$), with the correlation coefficient reaching its maximum ($R = 0.93$) between 420 and 440 nm (Fig. S8). The strong relationship across the entire absorbance spectrum indicates that the DOM concentration is the primary driver of differences between sites with DOM properties related to specific wavelengths contributing to the minor increase in R between 420 and 440 nm. Although small, the increase in correlation coefficient between 420 and 440 nm may indicate a specific loss of absorbance from photodegradation of residual pigments related to phytoplankton death or macroalgal exudation (Blough, 2001; Hulatt et al., 2009) or may merely be related to the unique behavior of W64 samples noted earlier (Fig. S3).

Because percent loss in absorbance at each wavelength was independent of DOM concentration, we also evaluated the relationship between percent MeHg loss and percent absorbance loss for each wavelength to identify possible wavelengths directly related to MeHg loss. Linear regressions between percent loss of MeHg and absorbance across the absorbance spectra showed maximum correlation coefficients ($R = 0.87$ to 0.88; $p < 0.001$) occurring throughout the range 280 to 350 nm and dropping off markedly above 400 nm (Fig. S8). The loss of absorbance in the range of 280 to 320 nm has been observed previously and attributed to photo-production of low molecular weight carbonyl compounds from direct photolytic cleavage of the C–C bonds in humic substances by UV-B energy (Kieber et al., 1990), suggesting a linkage between MeHg degradation and the photodegradation of these DOM structures.

Similar to absorbance, fluorescence data showed specific regions of the EEMs spectra strongly related to MeHg. Relationships between MeHg and fluorescence intensities were strongest in protein-like region of peak T and peak N associated with algal origin (Fig. 4A), whereas the region of peak C and FDOM were areas of the weakest correlation coefficients. The higher correlation between MeHg and fluorescence in peak T and peak N suggests that the higher MeHg concentrations are related to sites with more labile DOM and higher ecosystem productivity in general. More labile forms of DOM are known to stimulate the production of MeHg (Windham-Myers et al., 2009), at least until the point at which biodilution occurs (Karimi et al., 2007; Pickhardt et al., 2005). In contrast, the loss of MeHg was more strongly related to the loss of the humic or fulvic portion of the DOM across a wide area of the EEMs spectra (Fig. 4B). The highest correlation coefficients were observed to be in the longer wavelengths in the area of peak C and the FDOM region, an area attributed to quinoid humic structures (Cook et al., 2008). These humic regions are the same structures believed to be photodegraded to form OH radicals (Blough, 2001) and carbonyl compounds (Kieber et al., 1990) as noted above.

The relationships observed between MeHg and specific portions of the DOM in the previous analyses were verified using principal component analysis (PCA). The use of PCA also allowed for the comparison of the relative influence of the absorbance and fluorescence properties listed in Table 1 with respect to MeHg concentration (Fig. S9) and percent change in MeHg with light exposure (Fig. S10). The concentration-based analysis confirmed that primary differences were between sites (PC1) with a secondary difference occurring within sites (PC2) separated along the light exposure time series (Fig. S9A). Bulk DOM concentration (as DOC) dominated PC1 whereas differences in humic fluorescence peaks appeared to dominate PC2 (Fig. S9B). In contrast to the previous analyses, the indicators related to microbial or algal DOM (i.e. peak B, peak T, A_{440}) did not factor into the correlation loadings for the concentration-based analysis, suggesting that these attributes did not contribute to variation in the data (Fig. S9C). The use of PCA for the percent change over light exposure was not influenced by bulk DOM concentration (Fig. S10). In this analysis, data clustered by light exposure across sites with the dark bottles falling in the lower right quadrant and clear bottles with greatest light exposure clustering in the upper left quadrant (Fig. S10A). The primary components (PC1 and PC2) in this analysis (Fig. S10B) consisted of a far more complex mixture of fluorescent and absorbance properties than the concentration-based analysis (Fig. S9B). The correlation loading indicated a close positive relationship between percent change in MeHg with the percent change in absorbance in the UV range and humic regions of the EEM spectra and a negative relationship with spectral slopes and slope ratios illustrating the complex relationship between MeHg and DOM (Fig. S10C).

4. Conclusions

The photodegradation rate measured in this study (7.5 +/− 3.5 $m^2\ mol^{-1}$) was similar to previously reported rates for freshwater and estuarine systems. Despite a wide range in both DOM concentration and character, the photodegradation rate was a function of light exposure. High DOM concentrations were proposed to be responsible for relatively low MeHg degradation rates in some systems because the DOM attenuated the light, essentially shading MeHg within the water column (Li et al., 2010). In contrast, Black et al. (2012) observed only a small effect of DOM concentration on MeHg photodemethylation rates despite high attenuation of light in the water column, suggesting a complex role of DOM in demethylation.

ARTICLE IN PRESS

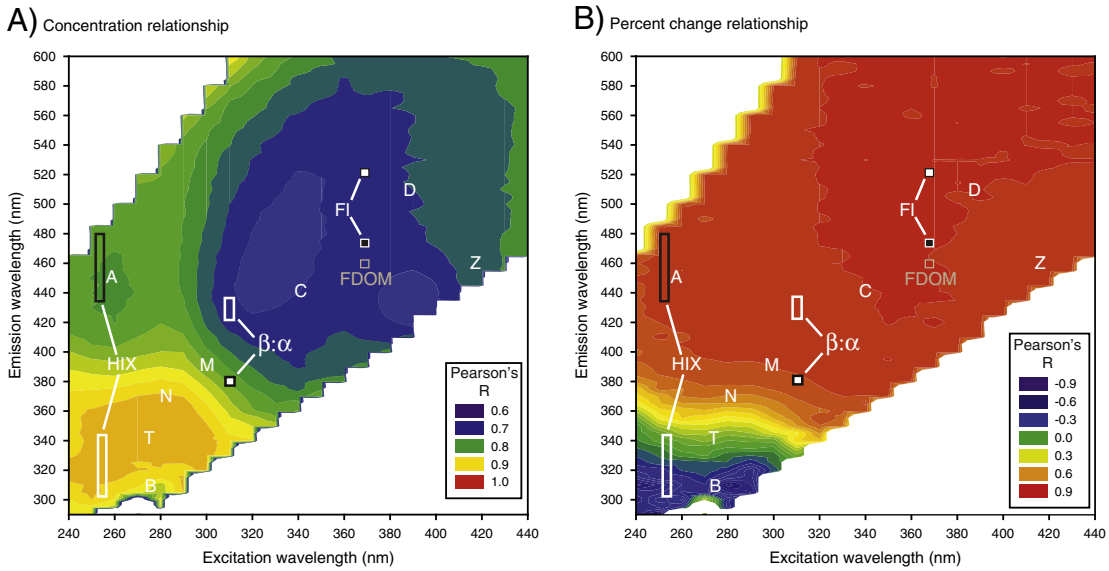

Fig. 4. Contour plots showing Pearson Product Moment correlation coefficients (Pearson's R) for each excitation–emission pair across the EEMs spectra. Figure A shows the correlation coefficients between MeHg concentration and fluorescence intensities. Figure B shows the correlation coefficients between the percent loss of MeHg and percent loss of fluorescence intensities.

The results in this study are more in line with those of Black et al. (2012), in that there was no observable effect of DOM concentration on photodemethylation rates over a large DOM concentration range (8 to 34 mg C L^{-1}) and a large ratio of MeHg to DOM (0.02 to 0.11 ng Hg mg C^{-1}). It is possible that this trend would change in more highly contaminated areas where higher ratios of MeHg (and Hg) to DOM affect binding conditions (Haizer et al., 2002; Zhang and Hsu-Kim, 2010).

The data shown here support the conclusion that DOM affects photodemethylation in complex ways that are not reflected in a simple relationship between DOM concentration and demethylation rates (Black et al., 2012). Results suggest photolytic reactions occur that affect specific regions across the absorbance and fluorescence spectra that represent different DOM components. Changes in the regions of the DOM optical spectra that were principally affected by light exposure are known to produce OH radicals (Blough, 2001), singlet oxygen ($\bullet O_2$) (Latch and McNeil, 2006), and DOM radicals (Brezonik, 1994). Although this correspondence could occur without a mechanistic relationship, the relationships observed between the loss of specific fluorescent DOM and MeHg in this study are provocative. The strong relationships between the percent loss of MeHg and percent loss of chromophoric DOM containing aromatic and/or quinoid humic structures suggest light exposure alters DOM moieties directly bound with MeHg, similar to what has been reported for the photoreduction of Hg^{II} (Gu et al., 2011; O'Driscoll et al., 2006). These data, particularly the relationship between percent loss of FDOM and MeHg during photolytic degradation, support the notion that light-induced reactions not only occur in the DOM sphere but are potentially linked to the binding site itself (Hines and Brezonik, 2004; Latch and McNeil, 2006; Zhang and Hsu-Kim, 2010).

The results of this study provide valuable information towards the understanding of MeHg photodemethylation and the relationship to DOM photodegradation in shallow flooded environments including areas of rice cultivation. Despite the complexity in the concurrent photolytic degradation of MeHg and DOM, demethylation appears to be driven primarily by cumulative exposure to solar radiation, therefore differences in photolytic degradation between aquatic systems will be driven more by physical factors such as shading by vegetation and particles within the water column and hydrologic controls on residence time than by chemical drivers. Differences in MeHg concentration between open water and vegetated areas may be more the result of limits on photodegradation processes than differences in net MeHg production processes in the sediment (Marvin-DiPasquale et al., in this issue; Windham-Myers et al., in this issue). Alternatively, the degradation of DOM to more labile forms may have an effect on MeHg production rates caused by the stimulation of microbial activity. Further research should focus on the relative importance of photodegradation as both a competitive and synergistic process in the net production of MeHg in vegetated and open water areas of wetlands, with optical measurements of DOM providing critical information about both processes.

Additionally, the results of this study provide valuable information about the relationships between photolytic degradation of both MeHg and DOM that may be used to develop tools to improve monitoring programs and aid the development of a regulatory framework for reducing MeHg exposure in aquatic systems. Optical measurements of DOM may provide a useful tool for understanding factors controlling MeHg photodemethylation in situ. Initial MeHg concentrations appear to be related to bulk DOM concentration and possibly indicators of DOM lability or general field productivity (T peak) whereas the loss of MeHg appears to be related more to the loss of specific humic structures within the DOM which fluoresce in the area of FDOM (Cory et al., 2010). Simple deduction would suggest that a ratio between optical indicators in these regions could provide the information necessary to identify MeHg concentration across both its production and loss, but no such diagnostic ratio was identified in this study. Further efforts should attempt to identify ratios within and between absorbance and fluorescence spectra that may capture the integrative effect of MeHg production and loss processes. Other measures of MeHg production such as iron and sulfur speciation or dissolved manganese concentration may help predict initial conditions that control initial MeHg–DOM relationships (Alpers et al., in this issue; Marvin-DiPasquale et al., in this issue).

Supplementary data to this article can be found online at http://dx.doi.org/10.1016/j.scitotenv.2013.03.107.

Acknowledgments

The authors would like to thank the staff at the USGS California Water Science Center in Sacramento, particularly Frank Anderson

and Liz Beaulieu for field and data support and Will Kerlin for laboratory support. We extend sincere appreciation to the California Department of Fish and Game staff at the Yolo Bypass Wildlife Management Area particularly Dave Feliz, Mary Schiedt, Waylon, Spencer, and Chris Rocco. We would also like to thank Yolo Basin Foundation staff Robin Kulako and Ann Brice and DeWit Farms staff for their cooperation and guidance on local history and rice production as well as for providing valuable information on site management. Base funding provided by Proposition 40 via California State Water Resources Control Board, additional funds provided by the USGS Cooperative Water Program. The use of brand or firm names in this article is for identification purposes only and does not constitute endorsement by United States Geological Survey. We greatly appreciate reviews by Dr. Edward Nater, Dr. Mae Gustin and several journal reviewers whose comments helped to improve this manuscript. The U.S. Geological Survey has approved this manuscript for publication.

References

Alpers CN, Fleck JA, Marvin-DiPasquale M, Stricker CA, Stephenson M. Mercury cycling in agricultural and managed wetlands, Yolo Bypass, California: spatial and seasonal variations in water quality. Sci Total Environ 2013e. [in this issue].

Baker A, Spencer RGM. Characterization of dissolved organic matter from source to sea using fluorescence and absorbance spectroscopy. Sci Total Environ 2004;333:217–32.

Bergamaschi BA, Fleck JA, Downing BD, Boss E, Pellerin B, Ganju NK, et al. Methyl mercury dynamics in a tidal wetland quantified using in situ optical measurements. Limnol Oceanogr 2011;56:1355–71.

Bergamaschi BA, Fleck JA, Downing BD, Boss E, Pellerin BA, Ganju NK, et al. Mercury dynamics in a San Francisco Estuary tidal wetland: assessing dynamics using in situ measurements. Estuar Coasts 2012. http://dx.doi.org/10.1007/s12237-012-9501-3.

Bergquist BA, Blum JD. Mass-dependent and independent fractionation of Hg isotopes by photo-reduction in aquatic systems. Science 2007;318:417–20.

Black FA, Poulin BA, Flegal AR. Factors controlling the abiotic photo-degradation of monomethylmercury in surface waters. Geochim Cosmochim Acta 2012;84:492–507.

Bloom N. Determination of picogram levels of methylmercury by aqueous phase ethylation followed by cryogenic gas chromatography with cold vapour atomic fluorescence detection. Can J Fish Aquat Sci 1989;46:1131–40.

Blough NV. Photochemical processes. Encycl Ocean Sci 2001:2162–72.

Blough NV, DelVecchio R. Chromophoric DOM in the coastal environment. In: Hansel DA, Carlson CA, editors. Biogeochemistry of marine dissolved organic matter. San Diego: Academic Press; 2002. p. 509–46.

Boss E, Zaneveld JRV. The effect of bottom substrate on inherent optical properties: evidence of biogeochemical processes. Limnol Oceanogr 2003;48:346–54.

Brezonik PL. Chemical kinetics and process dynamics in aquatic systems. Boca Raton, FL, USA: CRC Press, Lewis Publishers; 1994.

Brigham ME, Wentz DA, Aiken GR, Krabbenhoft DP. Mercury cycling in stream ecosystems. 1. Water column chemistry and transport. Environ Sci Technol 2009;43:2720–5.

Byington A. Photo-degradation of methylmercury in the Sacramento–San Joaquin Delta Estuary. Master of Science Thesis. San Jose, Calif.: San Jose State University and Moss Landing Marine Laboratory; 2007 [64 pp.].

Chen W, Westerhoff P, Leenheer JA, Booksh K. Fluorescence excitation–emission matrix regional integration to quantify spectra for dissolved organic matter. Environ Sci Technol 2003;37:5701–10.

Choe K-Y, Gill GA. Distributions of particulate, colloidal and dissolved mercury in the San Francisco Bay estuary: 2. Monomethyl mercury. Limnol Oceanogr 2003;48:1547–56.

Choe K-Y, Gill GA, Lehman RD. Distributions of particulate, colloidal and dissolved mercury in the San Francisco Bay estuary: 1. Total mercury. Limnol Oceanogr 2003;48:1535–46.

Coble PG. Characterization of marine and terrestrial DOM in seawater using excitation–emission matrix spectroscopy. Mar Chem 1996;52:325–36.

Coble PC, Green S, Blough NV, Gagosian RB. Characterization of dissolved organic matter in the Black Sea by fluorescence spectroscopy. Nature 1990;348:432–5.

Coble PG, Del Castillo CE, Avril B. Distribution and optical properties of CDOM in the Arabian Sea during the 1995 Southwest Monsoon. Deep-Sea Res II 1998;45:2195–223.

Cook RL, Birdwell JE, Lattao C, Lowry M. A Multi-method comparison of Atchafalaya basin surface water organic matter samples. J Environ Qual 2008;38:702–11.

Cory RM, McKnight DM. Fluorescence spectroscopy reveals ubiquitous presence of oxidized and reduced quinones in dissolved organic matter. Environ Sci Technol 2005;39:8142–9.

Cory R, Miller MP, McKnight DM, Guerard JJ, Miller PL. Effect of instrument-specific response on the analysis of fulvic acid fluorescence spectra. Limnol Oceanogr Methods 2010;8:67–78.

Cory RM, Boyer EW, McKnight DM. Spectral methods to advance understanding of dissolved organic carbon dynamics in forested catchments. In: Levia DF, et al, editor. Forest hydrology and biogeochemistry: synthesis of past research and future directions. Ecological StudiesSpringer Science+Business Media B.V.; 2011. http://dx.doi.org/10.1007/978-94-007-1363-5_6.

Crump KL, Trudeau VL. Mercury-induced reproductive impairment in fish. Environ Toxicol Chem 2009;28:895–907. http://dx.doi.org/10.1897/08-151.1.

Dalzell BJ, Minor EC, Mopper KM. Photodegradation of estuarine dissolved organic matter: a multi-method assessment of DOM transformation. Org Geochem 2009;40:243–57.

Del Vecchio R, Blough NV. Photobleaching of chromophoric dissolved organic matter in natural waters: kinetics and modeling. Mar Chem 2002;78:231–53.

Del Vecchio R, Blough NV. On the origin of the optical properties of humic substances. Environ Sci Technol 2004;38:3885–91.

Dittman JA, Shanley JB, Driscoll CT, Aiken GR, Chalmers AT, Towse JE. Ultraviolet absorbance as a proxy for total dissolved mercury in streams. Environ Pollut 2009;157:1953–6.

Dittman JA, Shanley JB, Driscoll CT, Aiken GR, Chalmers AT, Towse JE, et al. Mercury dynamics in relation to dissolved organic carbon concentration and quality during high flow events in three northeastern U.S. streams. Water Res 2010;46:W07522. http://dx.doi.org/10.1029/2009WR008351.

Downing BD, Boss E, Bergamaschi BA, Fleck JA, Lionberger MA, Ganju NK, et al. Quantifying fluxes and characterizing compositional changes of dissolved organic matter in aquatic systems in situ using combined acoustic and optical measurements. Limnol Oceanogr Methods 2009;7:119–31.

Engelhaupt E, Bianchi TS, Wetzel RG, Tarr MA. Photochemical transformations and bacterial utilization of high-molecular-weight dissolved organic carbon in a southern Louisiana stream (Bayon Trepagnier). Biogoechem 2003;62:39–58.

Gao H, Zepp RG. Factors Influencing photoreactions of dissolved organic matter in a coastal river of the southeastern United States. Environ Sci Technol 1998;32:2940–6.

Geological Survey US. Research in rice fields, Fact Sheet. . USGS FS-021-00 Junehttp://www.nwrc.usgs.gov/factshts/021-00.pdf2000.

Gerbig CA, Ryan JN, Aiken GR. The effects of dissolved organic matter on mercury biogeochemistry. In: Liu G, et al, editor. Environmental chemistry and toxicology of mercury. Hoboken, NJ, USA: John Wiley & Sons, Inc.; 2011. http://dx.doi.org/10.1002/9781118146644.

Gill GA, Fitzgerald WF. Mercury sampling in open ocean waters at the picomolar level. Deep Sea Res 1985;32:287–97.

Gilmour CC, Henry EA, Mitchell R. Sulfate stimulation of mercury methylation in freshwater sediments. Environ Sci Technol 1992;26:2281–7.

Gorski PR, Armstrong DE, Hurley JP, Krabbenhoft DP. Influence of natural dissolved organic carbon on the bioavailability of mercury to a freshwater alga. Environ Pollut 2008;154:116–23.

Graham AM, Aiken GR, Gilmour CC. Dissolved organic matter enhances microbial mercury ethylation under sulfidic conditions. Environ Sci Technol 2012;46:2715–23.

Gu Q, Kenny JE. Improvement of inner filter effect correction based on determination of effective geometric parameters using a conventional fluorimeter. Anal Chem 2009;81:420–6.

Gu B, Bian Y, Miller CL, Dong W, Jiang X, Liang L. Mercury reduction and complexation by natural organic matter in anoxic environments. Proc Natl Acad Sci 2011;108:1479–83.

Haizer M, Aiken GR, Ryan JN. Binding of mercury(II) to dissolved organic matter: the role of the mercury-to-DOM concentration ratio. Environ Sci Technol 2002;36:3564–70.

Hall BD, Aiken GR, Krabbenhoft DP, Marvin-DiPasquale M, Swarzenski CM. Wetlands as principal zones of methylmercury production in southern Louisiana and the Gulf of Mexico region. Environ Pollut 2009;154:124–34. http://dx.doi.org/10.1016/j.envpol.2007.12.017.

Hammerschmidt CR, Fitzgerald WF. Iron-mediated photochemical decomposition of methylmercury in an arctic Alaskan lake. Environ Sci Technol 2010;44:6138–43.

Hammerschmidt CR, Fitzgerald WF, Lamborg CH, Balcom PH, Tseng C-M. Biogeochemical cycling of methylmercury in lakes and tundra watersheds of arctic Alaska. Environ Sci Technol 2006;40:1204–11.

Han S, Gill GA, Lehman RD, Choe K-Y. Complexation of mercury by dissolved organic matter in surface waters of Galveston Bay, Texas. Mar Chem 2006;98:156–66.

Helms JR, Stubbins A, Ritchie JD, Minor EC, Kieber DJ, Mopper K. Absorption spectral slopes and slope ratios as indicators of molecular weight, source, and photobleaching of chromophoric dissolved organic matter. Limnol Oceanogr 2008;53:955–69.

Hernes PJ, Bergamaschi BA, Eckard RS, Spencer RGM. Fluorescence-based proxies for lignin in freshwater dissolved organic matter. J Geophys Res 2009;114:G00F03. http://dx.doi.org/10.1029/2009JG000938.

Hill JE, Williams JF, Mutters RG, Greer CA. The California rice cropping system: agronomic and natural resource issues for long-term sustainability. Paddy Water Environ 2006;4:13–9. http://dx.doi.org/10.1007/s10333-005-0026-2.

Hines NA, Brezonik PL. Mercury dynamics in a small northern Minnesota lake: water to air exchange and photoreactions of mercury. Mar Chem 2004;90:137–49.

Hintelmann H, Welbourn PM, Evans RD. Measurement of complexation of methylmercury(II) compounds by freshwater humic substances using equilibrium dialysis. Environ Sci Technol 1997;31:489–95.

Horvat M, Bloom NS, Liang L. A comparison of distillation with other current isolation methods for the determination of methyl mercury compounds in low level environmental samples. Part 2, water. Anal Chim Acta 1993;282:153–68.

Hulatt CJ, Thomas DN, Bowers DG, Norman L, Zhang C. Exudation and decomposition of chromophoric dissolved organic matter (CDOM) from some temperate macroalgae. Estuar Coast Shelf Sci 2009;84:147–53.

Karimi R, Chen CY, Pickhardt PC, Fisher NS, Folt CL. Stoichiometric controls of mercury dilution by growth. Proc Nat Acad Sci 2007;104:7477–82.

Khwaja AR, Bloom PR, Brezonik PL. Binding strength of methylmercury to aquatic NOM. Environ Sci Technol 2010;44:6151–6.

Kieber RJ, Zhou X, Mopper K. Formation of carbonyl compounds from UV-induced photodegradation of humic substances in natural waters: Fate of riverine carbon in the sea. Limnol Oceanogr 1990;35:1503–15.
Kieber RJ, Hydro LH, Seaton PJ. Photooxidation of triglycerides and fatty acids in seawater: implication toward the formation of marine humic substances. Limnol Oceanogr 1997;42:1454–62.
Kraus TEC, Anderson CA, Morgenstern K, Downing BD, Pellerin BA, Bergamaschi BA. Determining sources of dissolved organic carbon and disinfection by-product precursors to the McKenzie River, Oregon: use of absorbance and fluorescence spectroscopy. J Environ Qual 2010;39:2100–12. http://dx.doi.org/10.2134/jeq2010.0030.
Kritee K, Blum JD, Reinfelder JR, Barkay T. Microbial stable isotope fractionation of mercury: a synthesis of present understanding and future directions. Chem Geol 2012. http://dx.doi.org/10.1016/j.chemgeo.2012.08.017.
Lamborg CH, Tseng C-M, Fitzgerald WF, Balcom PH, Hammerschmidt CR. Determination of the mercury complexation characteristics of dissolved organic matter in natural waters with "reducible Hg" titrations. Environ Sci Technol 2003;37:3316–22.
Latch DE, McNeill K. Microheterogeneity of singlet oxygen distributions in irradiated humic acid solutions. Science 2006;311:1743–7.
Lehnherr I, St. Louis VL. Importance of ultraviolet radiation in the photodemethylation of methylmercury in freshwater ecosystems. Environ Sci Technol 2009;43:5692–8.
Lehnherr I, St Louis VL, Emmerton CA, Barker JD, Kirk JL. Methylmercury cycling in high arctic wetland ponds: sources and sinks. Environ Sci Technol 2012;46:10514–22.
Li Y, Mao Y, Liu G, Tachiev G, Roelant D, Feng X, et al. Degradation of methylmercury and its effects on mercury distribution and cycling in the Florida Everglades. Environ Sci Technol 2010;44:6661–6.
Marvin-DiPasquale M, Windham-Myers L, Agee JL, Kakouros E, Kieu LH, Fleck JA. Methylmercury production in sediment from agricultural and non-agricultural wetlands in the Yolo Bypass, California. Sci Total Environ 2013e. [in this issue].
McKnight DM, Boyer EW, Westerhoff PK, Doran PT, Kulbe T, Andersen DT. Spectrofluorometric characterization of dissolved organic matter for indication of precursor organic material and aromaticity. Limnol Oceanogr 2001;46:38–48.
Mergler D, Anderson HA, Chan LHM, Mahaffey KR, Murray M, Sakamoto M, et al. Methylmercury exposure and health effects in humans: a worldwide concern. Ambio 2007;36:3-11.
Minor EC, Dalzell BJ, Stubbins A, Mopper K. Evaluating the photoalteration of estuarine dissolved organic matter using direct temperature-resolved mass spectrometry and UV–visible spectroscopy. Aquat Sci 2007;69:440–55.
Merriam J, McDowell WH, Currie WS. A high-temperature catalytic oxidation technique for determining total dissolved nitrogen. Soil Sci Soc Am J 1996;60:1050–5.
Mitro MG, Evers DC, Meyer MW, Piper WH. Common loon survival rates and mercury in New England and Wisconsin. J Wildl Manag 2008;72:665–73.
Mopper K, Kieber DJ. Marine photochemistry and its impact on carbon cycling. In: de Mora SJ, Demers S, Vernet M, editors. The effects of UV radiation in the marine environment. Cambridge University Press; 2000. p. 109–12.
Moran MA, Zepp RG. Role of photoreactions in the formation of biologically labile compounds from dissolved organic matter. Limnol Oceanogr 1997;42:1307–16.
Mostafa KG, Yoshioka T, Konohira E, Tanoue E. Photodegradation of fluorescent dissolved organic matter in river waters. Geochem J 2007;41:323–31.
Nguyen ML, Westerhoff PPE, Baker L, Hu Q, Esparza-Soto M, Sommerfeld M. Characteristics and reactivity of algae-produced dissolved organic carbon. J Environ Eng 2005;131:1574–82.
O'Driscoll N, Siciliano SD, Peak D, Carignan R, Lean DRS. The influence of forestry activity on the structure of dissolved organic matter in lakes: implications for mercury photoreactions. Sci Total Environ 2006;366:880–93.
Ohno T. Fluorescence inner-filtering correction for determining the humification index of dissolved organic matter. Environ Sci Technol 2002;36:742–6.
Ohno T, Amirbahman A, Bro R. Parallel factor analysis of excitation–emission matrix fluorescence spectra of water soluble soil organic matter as basis for the determination of conditional metal binding parameters. Environ Sci Technol 2008;42:186–92. http://dx.doi.org/10.1021/es071855f.
Parlanti E, Worz K, Geoffroy L, Lamotte M. Dissolved organic matter fluorescence spectroscopy as a tool to estimate biological activity in a coastal zone submitted to anthropogenic inputs. Org Geochem 2000;31:1765–81.
Pickhardt PC, Fisher NS. Accumulation of inorganic and methylmercury by freshwater phytoplankton in two contrasting water bodies. Environ Sci Technol 2007;41:125–31.
Pickhardt PC, Folt CL, Chen CY, Klaue B, Blum JD. Impacts of zooplankton composition and algal enrichment on the accumulation of mercury in an experimental freshwater food web. Sci Total Environ 2005;339:89-101.
Qian J, Skyllberg U, Frech W, Bleam WF, Bloom PR, Petit PE. Bonding of methyl mercury to reduced sulfur groups in soil and stream organic matter as determined by X-ray absorption spectroscopy and binding affinity studies. Geochim Cosmochim Acta 2002;66:3873–85.
Ravichandran M. Interactions between mercury and dissolved organic matter — a review. Chemosphere 2004;55:319–31.
Romera-Castillo C, Nieto-Cid M, Castro CG, Marrasé C, Largier J, Barton ED, et al. Fluorescence:absorption coefficient ratio — tracing photochemical and microbial degradation processes affecting coloured dissolved organic matter in a coastal system. Mar Chem 2011;125:26–38.
Schuster PF, Striegl RG, Aiken GR, Krabbenhoft DP, Dewild JF, Butler K, et al. Mercury export from the Yukon River basin and potential response to a changing climate. Environ Sci Technol 2011;45:9262–7.
Selin NE. Global biogeochemical cycling of mercury: a review. Annu Rev Environ Res 2009;34:43–63. http://dx.doi.org/10.1146/annurev.environ.051308.084314.
Sellers P, Kelly CA, Rudd JWM, MacHutchon AR. Photodegredation of methylmercury in lakes. Nature 1996;380:694–7.
Sellers P, Kelly CA, Rudd JWM. Fluxes of methylmercury to the water column of a drainage lake: the relative importance of internal and external sources. Limnol Oceanogr 2001;46:623–31.
Shubina D, Fedoseeva E, Gorshkova O, Patsaeva S, Terekhova V, Timofeev M, et al. The "blue shift" of emission maximum and the fluorescence quantum yield as quantitative spectral characteristics of dissolved humic substances. EARSeL eProceedings 2010;9.
Spencer RGM, Pellerin BA, Bergamaschi BA, Downing BD, Kraus TEC. Diurnal variability in riverine dissolved organic matter composition determined by in situ optical measurement in the San Joaquin River (California, USA). Hydrol Process 2007;21:3181–9.
Spencer RGM, Stubbins A, Hernes PJ, Baker A and Mopper K. Photochemical degradation of dissolved organic matter and dissolved lignin phenols from the Congo River. J Geophys Res 2009;114, G03010. http://dx.doi.org/10.1029/2009JG000968.
St. Louis VL, Rudd JWM, Kelly CA, Beaty KG, Flett RJ, Roulet NT. Production and loss of methylmercury and loss of total mercury from boreal forest catchments containing different types of wetlands. Environ Sci Technol 1996;30:2719–29.
Stedmon CA, Markager S, Bro R. Tracing dissolved organic matter in aquatic environments using a new approach to fluorescence spectroscopy. Mar Chem 2003;82:239–54.
Stepanauskas R, Moran MA, Bergamaschi BA, Hollibaugh JT. Sources, bioavailability, and photoreactivity of dissolved organic carbon in the Sacramento–San Joaquin River Delta. Biogeochemistry 2005;74:131–49.
Tsui MTK, Finlay JC. Influence of dissolved organic carbon on methylmercury bioavailability across Minnesota stream ecosystems. Environ Sci Technol 2011;45:5981–7.
Twardowski MS, Boss E, Sullivan JM, Donaghay PL. Modeling the spectral shape of absorption by chromophoric dissolved organic matter. Mar Chem 2004;89:69–88.
U.S. Environmental Protection Agency. Method 415.3 determination of total organic carbon and specific UV absorbance at 254 nm in source water and drinking water, EPA Document #: EPA/600/R-05/055. http://www.epa.gov/microbes/Method%20415_3_Rev1_2_Final.pdf2005.
Weishaar JL, Aiken GR, Bergamaschi BA, Fram MS, Fuji R, Mopper K. Evaluation of specific ultraviolet absorbance as an indicator of the chemical composition and reactivity of dissolved organic carbon. Environ Sci Technol 2003;37:4702–8.
Wiener JG, Krabbenhoft DP, Heinz GH, Scheuhammer AM. Ecotoxicology of mercury. In: Hoffman, et al, editor. Handbook of ecotoxicology. 2nd ed. Boca Raton, Fla., USA: CRC Press; 2003. p. 409–63.
Wilson HF, Xenopoulos MA. Effects of agricultural land use on the composition of fluvial dissolved organic matter. Nat Geosci 2009;2:37–41. http://dx.doi.org/10.1038/NGEO391009.
Windham-Myers LM, Marvin-DiPasquale M, Krabbenhoft DP, Agee J, Cox M, Heredia-Middleton P, et al. Experimental removal of wetland emergent vegetation leads to decreased methylmercury production in surface sediment. J Geophys Res 2009;114:G00C05.
Windham-Myers L, Fleck JA, Ackerman JT, Marvin-DiPasquale M, Stricker CA, Heim WA, et al. Mercury cycling in agricultural and managed wetlands: a synthesis of methylmercury production, hydrologic export, and bioaccumulation from an integrated field study. Sci Total Environ 2013a. [in this issue-a].
Windham-Myers L, Marvin-DiPasquale M, Kakouros E, Agee JL, Kieu LH, Stricker CA, et al. Mercury cycling in agricultural and managed wetlands, Yolo Bypass, California: vegetation influences on methylmercury production, export, and bioaccumulation. Sci Total Environ 2013b. [in this issue-b].
Wood ML, Foe C, Cooke J, Louie SJ. Sacramento–San Joaquin Delta Estuary TMDL for methylmercury: staff report. Sacramento, Calif: Regional Water Quality Control Board — Central Valley Region; 2010a [April, 234 pp.].
Wood ML, Morris P, Cooke J, Louie SJ. Amendments to the Water Quality Control Plan for the Sacramento River and San Joaquin River basins for the control of methylmercury and total mercury in the Sacramento–San Joaquin Delta Estuary: staff report. Regional Water Quality Control Board — Central Valley Region; 2010b [April, 332 pp.].
Zhang T, Hsu-Kim H. Photolytic degradation of methylmercury enhanced by binding to natural organic ligands. Nat Geosci 2010;3:473–6. http://dx.doi.org/10.1038/ngeo892.
Zhang Y, van Dijk M, Liu M, Zhu G, Qin B. The contribution of phytoplankton degradation to chromophoric dissolved organic matter (CDOM) in eutrophic shallow lakes: field and experimental evidence. Water Res 2009;43:4685–97.
Zhao J, Cao W, Wang G, Yang D, Yang Y, Sun Z, et al. The variations in optical properties of CDOM throughout an algal bloom event. Estuar Coast Shelf Sci 2009;82:225–32.
Zheng W, Hintelmann H. Mercury isotope fractionation during photoreduction in natural water is controlled by its Hg/DOC ratio. Geochim Cosmochim Acta 2009;73:6704–15.
Zheng W, Hintelmann H. Isotope fractionation of mercury during its photochemical reduction by low-molecular-weight organic compounds. J Phys Chem A 2010;114:4246–53.